New U-Pb zircon age and petrogenesis of the plagiogranite, Troodos ophiolite, Cyprus

Yanhong Chen[a,b*], Yaoling Niu[a,b,c,d*], Fangyu Shen[b,c,d], Yajie Gao[c,e], Xiaohong Wang[c,d]

[a]*School of Earth Science and Resources, China University of Geosciences, Beijing100083, China*

[b]*Department of Earth Sciences, Durham University, Durham DH1 3LE, UK*

[c]*Laboratory for Marine Geology, Qingdao National Laboratory for Marine Science and Technology, Qingdao 266061, China*

[d]*Institute of Oceanology, Chinese Academy of Sciences, Qingdao 266071, China*

[e]*Research School of Earth Sciences, Australian National University, Canberra ACT 2601, Australia*

**Corresponding author:*

Yanhong Chen, Yaoling Niu

School of Earth Science and Resources

China University of Geosciences

Beijing 100083

China

E-mail: chenyh@cugb.edu.cn (Y. Chen); yaoling.niu@durham.ac.uk (Y. Niu)

Abstract

The Troodos ophiolite is a classic and is one of the most complete and best-studied ophiolites on Earth. However, there are few studies on the geochronology of the plagiogranite in the Troodos ophiolite. With the advancement of zircon U-Pb *in situ* dating method developed in recent decades, it is necessary to revisit the age of the plagiogranite. In this study, we carried out detailed petrography, zircon U-Pb dating and mineral compositional analysis for the plagiogranite. Our new zircon ages of ~ 90-91 Ma confirm the previous age data. Our findings also offer new perspectives on the petrogenesis of the Troodos plagiogranite. It is common that some of the Troodos plagiogranite outcrops show intense "epidotization". The Troodos plagiogranite can thus be divided into epidote-free plagiogranite and epidote plagiogranite. Zircons in the epidote plagiogranite have mottled texture with high contents of most elements (especially for P, Y, REEs, Nb and Ta), which differs distinctly from those in the epidote-free plagiogranite with a clean appearance and oscillatory zoning. The two types of zircons all having high Th/U ratio (0.25-1.46 with an average of 0.69) are consistent with being of magmatic origin. The texture and composition of zircons from the epidote plagiogranite suggest that they are crystallized from a highly dissolving agent that transforms existing minerals such as plagioclase and amphiboles while concentrating rare earth elements (REEs) and high field strength elements (HFSEs, including Nb, Ta, Ti, Zr, Hf, Th and U^{4+}) to precipitate accessory minerals

such as zircon and titanite as well as the more abundant epidote. The intergrowth of quartz and skeletal plagioclase together with the precipitation of zircon, titanite and epidote indicates that the highly dissolving agent is best understood as late-stage magmatic fluid or more likely supercritical fluid/melt whose nature and origin deserve further investigation.

Keywords: Zircon U-Pb age; plagiogranite; Troodos ophiolite; Cyprus

1. Introduction

Oceanic plagiogranite refers to felsic rocks such as diorite, quartz diorite, tonalite and trondhjemite found in gabbroic sections of the ocean crust (Coleman and Peterman, 1975; Coleman and Donato, 1979). They are volumetrically minor but widespread in the present-day ocean crust and many ophiolites. Their high concentration in accessory minerals such as zircon, apatite and titanite make them ideal for dating the emplacement ages of the ocean crust and ophiolite complexes (e.g., Mattinson, 1976; Tilton et al., 1981; Mukasa and Ludden, 1987; Ménot et al., 1988; Schwartz et al., 2005; Warren et al., 2005).

The Troodos ophiolite is considered as one of the most complete and best-studied ophiolites on Earth, though debate continues on its origin and tectonic setting (e.g., Gass, 1968; Miyashiro, 1973; Pearce and Robinson, 2010; Osozawa et al., 2012;

Regelous et al., 2014). The zircon U-Pb dating for the plagiogranite in the Troodos ophiolite using thermal ionization mass spectrometer (TIMS; Mukasa and Ludden, 1987) has been important for our knowledge on the age of the Troodos ophiolite. It is time to revisit this age using the advanced zircon U-Pb *in situ* dating method on multiple crystals with more data to provide statistically significant age and possible age variation. Importantly, the age data together with the texture and compositions of the coexisting minerals are anticipated to offer insights into the petrogenesis of the plagiogranite.

In this paper, we present new zircon Laser Ablation-Inductively Coupled Plasma-Mass Spectrometry (LA-ICP-MS) U-Pb age data for the plagiogranite of the Troodos ophiolite, and use these data, together with petrography and mineral geochemistry to offer a new perspective on the petrogenesis of the Troodos plagiogranite and the ophiolite emplacement.

2. Geological background and petrology of the plagiogranite

The Troodos ophiolite is located in the central part of the island of Cyprus in the eastern Mediterranean (Fig. 1 inset), and is characterized by having a complete Penrose-type sequence of marine sediments, pillow lavas, sheeted dykes, isotropic gabbros, layered gabbros and mantle harzburgitic tectonite (Gass, 1968; Coleman, 1977). Zircon U-Pb ages from the plagiogranite, Ar-Ar ages of lavas (arc tholeiite) and radiolarian biostratigraphy from umber beds (Mn-Fe hydroxides of seafloor

hydrothermal origin) indicate that the Troodos ophiolite formed around 90-92 Ma (Blome and Irwin, 1985; Mukasa and Ludden, 1987; Konstantinou et al., 2007; Osozawa et al., 2012).

The Troodos ophiolite is separated by the Arakapas Fault Zone to two connected parts: the Mount Olympus (the Troodos sensu stricto) in the north and the Limassol Forest area in the south. In the Mount Olympus area, the mantle harzburgitic tectonite is surrounded by plutonic rocks including wehrlite, websterite, gabbro and plagiogranite, and then by sheeted dyke complex overlain by extrusive lavas and sediments (Fig. 1). The lavas have previously been divided into tholeiitic and boninitic types (e.g., Pearce and Robinson, 2010; Regelous et al., 2014 and references therein). The plagiogranite, comprised of a group of felsic rocks including diorite, quartz diorite, tonalite and trondhjemite, generally occurs near the gabbro-sheeted dykes contact (Mukasa and Ludden, 1987; Freund et al., 2014; Anenburg et al., 2015; Marien et al., 2019) and is intruded by diabasic sills and dykes (Fig. 2a). Our samples were collected from a gabbro-plagiogranite body located to the north of the main ultramafic complex (Fig. 1). Most of the plagiogranite samples show pervasive "epidotization" (Figs. 2b, 3). According to the presence of epidote in the plagiogranite, we divided these samples into epidote plagiogranite and epidote-free plagiogranite. This outcrop shows the gabbro, epidote plagiogranite and epidote-free plagiogranite in complex juxtaposition. Weathering of the outcrop makes it more difficult to ascertain the relationship between different lithologies.

The epidote-free plagiogranite sample is tonalite with quartz (~30%), plagioclase (~20%) and amphibole (~50%) (TDS18-08B; Figs. 2c and 3a, b). The epidote plagiogranite samples (TDS06 and TDS18-49) mainly consist of quartz, epidote and plagioclase (Fig. 3c-i) with higher quartz contents (~40-50%) than in the epidote-free plagiogranite sample (TDS18-08B). Plagioclase crystals in the epidote plagiogranite samples are euhedral to subhedral with albite twinning, and most of them have been partially altered to clays (Fig. 3c-i). Granophyric texture (i.e., intergrowth of angular plagioclase in quartz) is common in the epidote plagiogranite samples (Fig. 3c). Minor clinopyroxene is locally present and is partially transformed into chlorite (Fig. 3d). The epidotes are generally anhedral or aggregates coexisting with plagioclase and quartz (Fig. 3d-f). Accessory minerals such as apatite, zircon and titanite are common in the epidote plagiogranite samples (Fig. 3). Apatite occurs as fine needlelike inclusions widely distributed within quartz in most samples (Fig. 3c). Zircons are usually subhedral in the epidote plagiogranite samples showing anhedral shape (Fig. 3g, h) surrounding by epidote. Titanite is subhedral-anhedral along edges of plagioclase and quartz grains (Fig. 3d, e) or coexisting with epidote (Fig. 3i) in the epidote plagiogranite samples.

3. Analytical methods

Zircons from these three samples were separated for U-Pb dating using a combined method of heavy liquid and magnetic separation. Zircon grains were handpicked

under a binocular and mounted in epoxy, polished to expose grain interiors. Cathodoluminescence (CL) images were taken for inspecting internal structures of individual zircon grains and then selecting spots for U-Pb isotope analysis. Zircon U-Pb dating was conducted using Agilent 7900 inductively coupled plasma-mass spectrometer with a Photon Machines Excite 193 nm excimer Ar-F laser system at the Laboratory of Ocean Lithosphere and Mantle Dynamic (LOLMD), Institute of Oceanology, Chinese Academy of Science. A laser spot size of 35 μm, laser energy density of 3.31 J/cm^2 and a repetition rate of 6 Hz were applied for analysis. The detailed operating conditions for the laser sampling system and the ICP-MS instrument were described by Xiao et al. (under review). Each analysis includes 25 s background acquisition (gas blank) followed by 50 s data acquisition. Zircon 91500 was used as an external standard for U-Pb dating, and every five sample analyses were followed by analyzing zircon 91500 twice. Trace element compositions of zircons were calibrated against NIST 610 as external standard combined with ^{91}Zr as internal standardization (Liu et al., 2010a). The raw data of zircon U-Pb ages and trace elements were processed using ICPMSDataCal_ver12.0 (Liu et al., 2010b). Concordia diagrams and weighted mean calculations were carried out using Isoplot/Ex_ver4 (Ludwig, 2012).

Major and trace elements of epidote and titanite in sample TDS06 were analyzed in thin sections using LA-ICP-MS at the LOLMD. Most samples were analyzed using an 85 μm spot size, and few samples were analyzed using 40-65 μm spot size depending

on crystal size. Fractures and inclusions were carefully avoided. Laser energy density of 10.61 J/cm^2 at a repetition rate of 8 Hz were applied. USGS reference rock glasses (BCR-2G, BHVO-2G and BIR-1G) were used as external standards for calibration following Liu et al. (2008). Every five sample analyses were followed by an analysis of NIST 610 and GSE-1G (NIST 610 were used to correct for the time-dependent drift of sensitivity and mass discrimination). The raw data were processed using ICPMSDataCal_ver12.0 (Liu et al., 2008; Chen et al., 2011). Data quality was assessed by repeated analyses of GSE-1G over the analytical session. Overall precision and accuracy are generally better than 5% for major elements except for P_2O_5 (14%), and better than 10% for trace elements.

For bulk-rock geochemical analysis, all suspicious surface contaminants such as weathered surfaces, pen marks and saw marks of samples TDS06 and TDS18-49 were removed. The samples were then reduced to chips and ultrasonically cleaned in Milli-Q water before being dried and grinded into powder using agate mill in a clean environment. Bulk-rock major and trace elements were analyzed at the LOLMD, using an Agilent-5100 inductively coupled plasma-optical emission spectrometer (ICP-OES) and ICP-MS, respectively. USGS reference standards BCR-2, AGV-2 and GSP-2 were used to monitor the analytical accuracy and precision. Analytical precisions are better than 5% for most elements. Sample digestion and analytical details are given in Kong et al. (2019) and Chen et al. (2017).

4. Results

4.1. Textures and zircon U-Pb ages

Three plagiogranite samples from the Troodos ophiolite were selected for LA-ICP-MS zircon U-Pb dating, including an epidote-free plagiogranite (TDS18-08B) and two epidote plagiogranite samples (TDS06 and TDS18-49). Representative CL images of analyzed zircons are shown in Fig. 4. The zircon U-Pb isotope data are plotted on the Concordia diagram in Fig. 5 and listed in Supplementary Table S1.

Zircons of the epidote-free plagiogranite sample are euhedral to subhedral prismatic crystals with clear prisms and pyramids. They have varying grain size (60-200 μm) with aspect ratios of 2:1 to 4:1. They are transparent with few inclusions in transmitted light, and most of them display oscillatory zoning (Fig. 4a). Zircons from the epidote plagiogranite samples have distinct appearance with euhedral to anhedral tetragonal-dipyramid or stubby tetragonal prism shapes (50-160 μm in length) and irregular or pitted surfaces. They are translucent with inclusions in transmitted light, and all of them show mottled textures with or without oscillatory zoning (Fig. 4b, c).

Though these zircons differ in morphology and appearance, they show similar ages. After rejecting discordant ages, zircons from these three samples give similar weighted mean $^{206}Pb/^{238}U$ ages: 91.0 ± 0.4 Ma (MSWD = 0.97, n = 41) for sample TDS18-08B; 91.8 ± 0.7 Ma (MSWD = 1.14, n = 27) for sample TDS06; 90.1 ± 0.9 Ma (MSWD = 3.40, n = 36) for sample TDS18-49 (Fig. 5).

184 4.2. Mineral compositions

185 4.2.1. Zircon

186 Trace element compositions of the zircons are given in Supplementary Table S2.
187 All of these zircons of the epidote-free (TDS18-08B) and epidote (TDS06 and
188 TDS18-49) plagiogranite samples show positive Ce anomalies and negative Eu
189 anomalies (Fig. 6a, c, e). The Ce/Ce* (= $Ce_{OCN}/\sqrt{La_{OCN} \times Pr_{OCN}}$, the subscript
190 indicates ocean crust normalization, Niu and O'Hara, 2003) ratios of zircons in the
191 epidote-free plagiogranite sample (2.2-33.1) are lower than those of the epidote
192 plagiogranite sample (4.9-207.7). There are no obvious differences in zircons between
193 the epidote-free (TDS18-08B) and epidote (TDS06 and TDS18-49) plagiogranite
194 samples in terms of elemental patterns (Fig. 6), but zircons of the epidote
195 plagiogranite show significantly higher abundances of most elements (especially for P,
196 Y, REEs, Nb and Ta) relative to those of the epidote-free plagiogranite (Fig. 7).
197 Besides, Th/U and Nb/Ta ratios of zircons in the epidote plagiogranites show
198 variations of 0.4-1.6 and 1.7-5.7, which are higher than those of zircons in the
199 epidote-free plagiogranite (ranging of 0.3-0.9 and 1.1-2.9, respectively).

200 4.2.2. Epidote

201 Major and trace element compositions of epidote in sample TDS06 are given in
202 Supplementary Table S3. The over two orders of magnitude variation in REE
203 abundances from this single sample (Fig. 8a, c) indicates millimeter-scale or

204 microscopic scale compositional heterogeneity in the medium from which epidote
205 being crystallized, which is to a large extent controlled by elemental competition
206 among coexisting and/or co-precipitating phases (Fig. 3). All the epidotes crystals
207 analyzed show similar REE patterns with small varying $(La/Pr)_{OCN}$ ratio (1.1-2.9), but
208 large varying Eu anomalies (Eu/Eu* = 0.1-13.8; Figs. 8a, 9a). Epidotes with high REE
209 abundances tend to have negative Eu anomalies, whereas those with low REE
210 abundances tend to have positive Eu anomalies, reflecting the effect, or lacking the
211 effect, of plagioclase REE characteristics with very low REE levels and large positive
212 Eu anomalies. This "plagioclase" effect in the epidote composition is likely controlled
213 by two factors: (1) inheritance from prior (transformed from) plagioclase and (2)
214 crystallization in the vicinity of plagioclase depleted in plagioclase constituents (low
215 REEs and positive Eu anomalies) because of inefficient diffusion on microscopic
216 scales in a single thin section.

217 4.2.3. Titanite

218 Major and trace element compositions of titanite in sample TDS06 are given in
219 Supplementary Table S4. Again, similar to compositional variation of epidotes (Fig.
220 8a, c), the over one order of magnitude variation in REE abundances from this single
221 sample (Fig. 8b, d) points to millimeter-scale and microscopic scale compositional
222 heterogeneity in the medium from which titanite being crystallized, largely controlled
223 by elemental competition of the coexisting and/or co-precipitating phases (Fig. 3).
224 Most of these titanites show negative Eu anomalies, and a few shows slightly LREE

enriched REE patterns with varying $(La/Pr)_{OCN}$ ratio (0.2-2.5) and positive Eu anomalies (Eu/Eu* = 1.1-1.4) (Fig. 8b). Similar to epidotes, the Eu/Eu* ratios of the titanite show negative correlation with REE contents (Fig. 9b), which reflects the very "plagioclase" effect discussed above. In addition, the positive correlation between REE and Zr in the titanite may suggest the "zircon" effect (Fig. 9c). Titanites also have high contents of high field strength elements (HFSEs) such as Nb, Ta, Zr and Hf as expected (Figs. 8d, 9c, d).

4.3 Bulk-rock major and trace elements

Major and trace element compositions of the epidote plagiogranite samples are given in Supplementary Table S5. Samples TDS06 and TDS18-49 are granitic rocks with high SiO_2 (>65 wt%) and Al_2O_3 (>12 wt%), low MgO (<4 wt%) contents. Both of these two samples show depletion in LREE ($[Ce/Yb]_{OCN}$ = 0.3 and 0.4) with slightly La enrichment ($[La/Pr]_{OCN}$ > 1), and high Nb and Ta relative to LREEs (Fig. 10c, d). Sample TDS06 shows a positive Eu anomaly (Eu/Eu* = 1.2), while sample TDS18-49 shows a negative Eu anomaly (Eu/Eu* = 0.7) (Fig. 10a).

5. Discussion

5.1. Origin of the two types of zircon

To better understand the origin of these zircons (Fig. 4), we summarized our observations (including petrology, morphology, geochemistry and chronology) on

zircons of these three samples in Table 1. All these plagiogranite samples give consistent zircon weighted mean $^{206}Pb/^{238}U$ ages within error (Fig. 5). The host rock type, euhedral shape, oscillatory zoning with Th/U ratios of 0.3-0.9 indicate that zircons of the epidote-free plagiogranite sample (TDS18-08B) are of magmatic origin (Rubatto, 2002; Corfu et al., 2003; Hoskin and Schaltegger, 2003). The higher Th/U ratios of zircons of the epidote plagiogranite samples (TDS06 and TDS18-49) suggest that they are also of magmatic origin (e.g., Rubatto, 2002; Hoskin and Schaltegger, 2003; Kirkland et al., 2015). Their morphology, texture, and composition are distinct from zircons of epidote-free plagiogranite (Figs. 4, 7 and 11; Table 1), indicating that they formed under different physical and chemical conditions (i.e., crystallized from different magmas).

Though zircon ($ZrSiO_4$) is a stoichiometrically simple accessory mineral in rocks, it can incorporate significant minor and trace elements such as Sc, Y, REE, Ti, Hf, Th, U, Nb, Ta and P (Hanchar and Westrenen, 2007). Zircons, once formed, can preserve substantial chemical and isotopic information (Finch and Hanchar, 2003). The composition of zircons thus records information on their growing processes and histories. Like other minerals, the composition of zircons depends on (1) the composition of parental medium; (2) the elemental compatibility in zircons; (3) the coexisting and co-crystallizing minerals in competition with zircon for preferred chemical elements.

Zircons of the epidote plagiogranite show similar elemental patterns (Fig. 6) but

have significantly higher abundances of most elements (especially for P, Y, REEs, Nb and Ta) than zircons of the epidote-free plagiogranite (Fig. 7), and also have higher Th/U and Nb/Ta ratios, and lower Eu/Eu* value (Fig. 11a-c). The wide compositional range of zircons from the epidote plagiogranite (Fig. 11 and Table S2) in a single hand-specimen sample or thin-section indicates millimeter to microscopic scale heterogeneity largely controlled by elemental concentration gradient towards or away from existing crystals due to inefficient elemental diffusion at the time of crystallization and growth of minerals of interest (i.e., zircon, titanite, epidote).

The mottled or spotted texture in zircons of the epidote plagiogranite (Fig. 4b, c) could be interpreted as earlier formed magmatic zircons being corroded by a corrosive fluids associated with the epidote alteration, but this is unlikely because (1) corrosion would not simply cause the spotted crystal interiors, but should also cause corroded crystal edges, which is not observed (Fig. 4); (2) the elemental makeups of the two types of zircons are distinct (Fig. 7), and thus must have formed from compositionally different media in the first place. The mottled or spotted texture (Fig. 4), the distinctively different composition (Fig. 7) and the close association with abundant epidote mean that zircons of the plagiogranite with pervasive "epidotization" must have formed from the same medium that precipitated epidote crystals. This inference is consistent with and supported by the petrography that zircon and epidote coexist, and most zircon grains are enclosed by epidote aggregate (Fig. 3g, h). We further infer that the mottled or spotted zircon interiors are crystal "flaws" resulting from fast

crystallization and inhomogeneous elemental diffusion.

The above analysis, together with the petrography and zircon compositional data, leads to the conclusion that the epidote plagiogranite resulted from magmatic fluids or hydrous melts, but more likely under supercritical conditions with vapor + fluid + melt as a single phase. Such a supercritical fluid can have highly dissolving power to transform the existing minerals (e.g., amphibole and plagioclase) and transport REEs and HFSEs to precipitate to produce accessory minerals like zircon, apatite and titanite as well as pervasive epidotization (see below).

5.2. Origin of epidote and titanite in the epidote plagiogranite

Epidote plagiogranite is common in the Troodos ophiolite (Mukasa and Ludden, 1987; Freund et al., 2014; Anenburg et al., 2015; Marien et al., 2019). Epidote in the plagiogranite samples occurs as aggregates enclosing plagioclase and quartz (Fig. 3f, h, i) or altered from plagioclase (Fig. 3e). The irregular boundaries between epidote and plagioclase relic (Fig. 3d-i) indicate that the plagioclase has been dissolved by a highly dissolving medium (hydrous melts or fluid) and partially transformed into epidote. Most of the titanites in the epidote plagiogranite samples occurs either between epidotes and other minerals or enclosed by epidote with anhedral shape (Fig. 3g-i). Their close association with epidotes (Fig. 3g-i) implies that they must have also co-precipitated from the same dissolving medium.

For epidote ($Ca_2Al_2[Fe^{3+}, Al][SiO_4][Si_2O_7]O[OH]$) and titanite ($CaTiSiO_5$), Ca is an essential constituent, and it is concentrated in plagioclase and amphibole which are

major components in the plagiogranite. Dissolving most of the plagioclase and amphibole result in precipitating epidote and titanite in the epidote plagiogranite (Figs. 2b, 3c-i). The “plagioclase” effect in the epidote and titanite (Fig. 9a, b) confirms that plagioclase plays an important role in crystallizing these minerals. In addition, the existence of titanite, as well as mottled zircon in the epidote plagiogranite, indicates that the dissolving medium they precipitated from has the power of transporting REEs and HFSEs (including Ti, Zr, Hf, Nb, Ta, Th and U^{4+}). Compositional heterogeneity of epidote, titanite as well as zircon in millimeter to microscopic scale (Figs. 8, 9, 11) suggests inefficient elemental diffusion during their crystallization.

It is usually considered that the pervasive epidotization in the Troodos plagiogranite is a result of hydrothermal alteration by seawater after solidification (e.g., Freund et al., 2014). Previous studies found that brine-rich aqueous fluids entrapped in quartz and epidote at temperatures >450-600 ℃ in the Troodos plagiogranite may originate from separation of an exsolved magmatic fluid (Kelley and Robinson, 1990; Kelley et al., 1992). A recent study focused on epidote in the plagiogranite proposed that the plagiogranite was epidotized by the means of its own exsolved magmatic fluids which was called autometasomatism (Anenburg et al., 2015). In our study, we find that (1) titanite and mottled zircon are closely related to epidote; (2) all of these minerals show wide compositional variation; (3) the mottled zircon shows higher Th/U, Nb/Ta and elemental abundances than those in the epidote-free plagiogranite. So, we propose that the epidote, titanite and mottled zircon are precipitated from the same highly

328 dissolving medium which is most likely hydrous melt or magmatic fluid under their
329 supercritical conditions. It dissolves and transforms existing minerals such as
330 plagioclase and amphibole, concentrating REEs and HFSEs, to precipitate zircon,
331 titanite and a large amount of epidote.

332 Such pervasive “epidotization” of plagiogranite is absent in the present-day ocean
333 crust (e.g., oceanic plagiogranite of Southwest Indian Ridge in ODP Hole 735B, Niu
334 et al., 2002; Chen et al., 2019). Compared with the supra-subduction setting, volatile
335 (such as water) component is usually depleted in basaltic magma in the mid-ocean
336 ridge setting, which makes it unlikely to produce epidote-rich plagiogranite without
337 allowing the development of supercritical melts/fluids.

338 5.3. Petrogenesis of plagiogranite of the Troodos ophiolite

339 It is proposed that plagiogranite can form by partial melting of hydrated gabbros
340 (Flagler and Spray, 1991; Koepke et al., 2004, 2007) and fractional crystallization at a
341 late stage of basaltic magma evolution (Coleman and Donato, 1979; Coleman and
342 Peterman, 1975; Niu et al., 2002; Chen et al., 2019). Detailed studies on the bulk rock
343 composition of the plagiogranite of Troodos ophiolite suggest that the plagiogranite is
344 formed by fractional crystallization of basaltic melt (Freund et al., 2014; Marien et al.,
345 2019). The U-Pb age of zircons from the plagiogranite samples in this study
346 (TDS18-08B: 91.0 ± 0.4 Ma; TDS06: 91.8 ± 0.4 Ma; TDS18-49: 90.1 ± 0.7 Ma)
347 represents the age of plagiogranite crystallization, which confirms the U-Pb zircon
348 ages of plagiogranite (between 90.3 ± 0.7 and 92.4 ± 0.7 Ma) analyzed using

whole-zircon (TIMS; Mukasa and Ludden, 1987). The similar U-Pb age but different compositional features of zircons from the epidote-free plagiogranite and the epidote plagiogranite samples suggest multiple intrusions and differentiations of plagiogranite in the Troodos ophiolite.

With continuous differentiation of basaltic melt, volatiles such as H_2O will be concentrated in the late-stage SiO_2-rich melt and become saturated (Fig. 12a). The intergrowths of quartz and skeletal plagioclase in the epidote plagiogranite samples (Fig. 3c) implies locally increased P_{H2O} (Smith, 1974). This hydrous melt or magmatic fluid is supercritical (Fig. 12a) with lower viscosity and highly dissolving power to dissolve and transport all the chemical elements including REEs and HFSEs. With the progressive concentration of SiO_2, Zr and REEs, zircons will become saturated to crystallize. Dissolution of plagioclase (Fig. 3e) and amphiboles will also lead to precipitation of epidote and titanite (Fig. 12b). Further studies are needed to constrain the stability and behavior of such medium of supercritical property.

Plagiogranites in the Mount Olympus area have been suggested to have compositionally different two groups (Freund et al., 2014; Marien et al., 2019): Main Group, produced by extensive fractional crystallization of tholeiitic melt; and Spilia Group, generated by fractional crystallization of boninitic melt. The epidote plagiogranite samples in this study show similar compositions to the Spilia Group with stronger depletion in LREE (Fig. 10). However, most of boninite (radiolarians and other fossils from conformably overlying sediments yielded ages of

approximately 75 Ma; some yielded an Ar-Ar age of 55.5 ± 0.9 Ma) in the Troodos ophiolite are considered to be formed later than the lower tholeiite (Ar-Ar age of 90.6 ± 0.7 Ma; Osozawa et al., 2012). Our new U-Pb zircon age suggests that this Spilia Group plagiogranite and lower tholeiite are contemporary. In addition, it is unlikely that boninitic magma can evolve to produce REE and HFSE-rich fluids with saturation of zircon and titanite (like sample TDS06 and TDS18-49 in this study), because boninite is characterized by low TiO_2 content (< 0.5 wt%; Le Bas, 2000) and depletion in HFSE (e.g., Nb, Ta, and Hf; Piercey et al., 2000).

6. Conclusions

We present new zircon LA-ICP-MS U-Pb age data, petrography and mineral geochemistry on the plagiogranite of the Troodos ophiolite. The zircon U-Pb age data give plagiogranite formation age of ~ 90-91 Ma, which confirms previous studies. Some of the Troodos plagiogranites have abundant epidotes. The zircons in epidote-rich plagiogranites show mottled or spotty textures, have high Y, REE, Nb, Ta, P and Th/U, which together with the intergrowths of quartz and skeletal plagioclase, and the abundant epidote and titanite, indicate that the epidote plagiogranite must have formed from crystallization of a highly dissolving agent, which is consistent with being of hydrous melt or magmatic fluid under supercritical conditions in order to explain all the mineral compositional data and texture characteristics. The detailed nature and origin of such supercritical fluids deserve further investigation for better

understanding the plagiogranite as a consequence of mafic magma evolution in a global context. We note that plagiogranite with varied mineralogical and chemical properties may vary as a function of tectonic setting.

Acknowledgments

We thank the company of Iain Neill, Peter Tollan and Durham 3rd year students during our annual Troodos field trips. We thank Dr. Xin Dong for her suggestions that helped to improve the paper. We thank Editor Xian-Hua Li for handling this manuscript and Prof. Wolfgang Bach and anonymous reviewer for constructive comments and suggestions. This study is supported by the National Nature Science Foundation of China (41130314, 41630968), Chinese Academy of Sciences Innovation (Y42217101L), grants from Qingdao National Laboratory for Marine Science and Technology (2015ASKJ03), the NSFC-Shandong Joint Fund for Marine Science Research Centers (U1606401) and 111 Project (B18048).

References

Anenburg, M., Katzir, Y., Rhede, D., Jöns, N., Bach, W., 2015. Rare earth element evolution and migration in plagiogranites: a record preserved in epidote and allanite of the Troodos ophiolite. Contributions to Mineralogy and Petrology 169(3), 25.

Blome, C. D., Irwin, W. P., 1985. Equivalent radiolarian ages from ophiolitic terranes

of Cyprus and Oman. Geology 13(6), 401-404.

Chen, L., Liu, Y., Hu, Z., Gao, S., Zong, K., Chen, H., 2011. Accurate determinations of fifty-four major and trace elements in carbonate by LA–ICP-MS using normalization strategy of bulk components as 100%. Chemical Geology 284(3-4), 283-295.

Chen, S., Wang, X.H., Niu, Y.L., Sun, P., Duan, M., Xiao, Y.Y., Guo, P.Y., Gong, H.M., Wang, G.D., Xue, Q.Q., 2017. Simple and cost-effective methods for precise analysis of trace element abundances in geological materials with ICP-MS. Science Bulletin 62, 277-289.

Chen, Y., Niu, Y., Wang, X., Gong, H., Guo, P., Gao, Y., Shen, F., 2019. Petrogenesis of ODP Hole 735B (Leg 176) oceanic plagiogranite: Partial melting of gabbros or advanced extent of fractional crystallization?. Geochemistry, Geophysics, Geosystems 20, 2717-2732.

Coleman, R.G., 1977. Ophiolites. Springer Verlag, New York.

Coleman, R.G., Donato, M.M., 1979. Oceanic plagiogranite revisited, in: Barker, F. (Ed.), Developments in Petrology. Elsevier, Amsterdam, Netherlands, vol. 6, pp. 149–168.

Coleman, R.G., Peterman, Z.E., 1975. Oceanic plagiogranite. Journal of Geophysical Research 80(8), 1099-1108.

Corfu, F., Hanchar, J.M., Hoskin, P.W., Kinny, P., 2003. Atlas of zircon textures. Reviews in mineralogy and geochemistry 53(1), 469-500.

Driesner, T., Heinrich, C.A., 2007. The system H2O–NaCl. Part I: Correlation formulae for phase relations in temperature–pressure–composition space from 0 to 1000°C, 0 to 5000 bar, and 0 to 1 XNaCl. Geochimica et Cosmochimica Acta 71(20), 4880-4901.

Finch, R.J., Hanchar, J.M., 2003. Structure and chemistry of zircon and zircon-group minerals. Reviews in mineralogy and geochemistry 53(1), 1-25.

Flagler, P.A., Spray, J.G., 1991. Generation of plagiogranite by amphibolite anatexis in oceanic shear zones. Geology 19(1), 70–73.

Freund, S., Haase, K.M., Keith, M., Beier, C., Garbe-Schönberg, D., 2014. Constraints on the formation of geochemically variable plagiogranite intrusions in the Troodos Ophiolite, Cyprus. Contributions to Mineralogy and Petrology 167(2), 978.

Gass, I. G., 1968. Is the Troodos massif of Cyprus a fragment of Mesozoic ocean floor?. Nature 220(5162), 39.

Gualda, G.A., Ghiorso, M.S., Lemons, R.V., Carley, T.L., 2012. Rhyolite-MELTS: a modified calibration of MELTS optimized for silica-rich, fluid-bearing magmatic systems. Journal of Petrology 53(5), 875-890.

Hanchar, J.M., Van Westrenen, W., 2007. Rare earth element behavior in zircon-melt systems. Elements 3(1), 37-42.

Hoskin, P.W., Schaltegger, U., 2003. The composition of zircon and igneous and metamorphic petrogenesis. Reviews in mineralogy and geochemistry 53(1),

27-62.

Kelley, D.S., Robinson, P.T., 1990. Development of a brine-dominated hydrothermal system at temperatures of 400–500°C in the upper level plutonic sequence, Troodos ophiolite, Cyprus. Geochimica et Cosmochimica Acta 54(3), 653-661.

Kelley, D.S., Robinson, P.T., Malpas, J.G., 1992. Processes of brine generation and circulation in the oceanic crust: fluid inclusion evidence from the Troodos ophiolite, Cyprus. Journal of Geophysical Research: Solid Earth 97(B6), 9307-9322.

Kirkland, C.L., Smithies, R.H., Taylor, R.J.M., Evans, N., McDonald, B., 2015. Zircon Th/U ratios in magmatic environs. Lithos 212, 397-414.

Koepke, J., Berndt, J., Feig, S.T., Holtz, F., 2007. The formation of SiO2-rich melts within the deep oceanic crust by hydrous partial melting of gabbros. Contributions to Mineralogy and Petrology 153(1), 67–84.

Koepke, J., Feig, S.T., Snow, J., Freise, M., 2004. Petrogenesis of oceanic plagiogranites by partial melting of gabbros: an experimental study. Contributions to Mineralogy and Petrology 146(4), 414–432.

Kong, J.J., Niu, Y.L., Sun, P., Xiao, Y.Y., Guo, P.Y., Hong, D., Zhang, Y., Shao, F.L., Wang, X.H., Duan, M., 2019. The origin and geodynamic significance of the Mesozoic dykes in eastern continental China. Lithos 332-333, 328-339.

Konstantinou, A., Wirth, K.R., Vervoort, J., 2007. October. U-Pb isotopic dating of Troodos plagiogranite, Cyprus by LA-ICP-MS. In 2007 GSA Denver Annual

Meeting (Vol. 28, p. 31).

Le Bas, M.J., 2000. IUGS reclassification of the high-Mg and picritic volcanic rocks. Journal of Petrology 41(10), 1467-1470.

Liu, Y., Gao, S., Hu, Z., Gao, C., Zong, K., Wang, D., 2010b. Continental and oceanic crust recycling-induced melt–peridotite interactions in the Trans-North China Orogen: U–Pb dating, Hf isotopes and trace elements in zircons from mantle xenoliths. Journal of Petrology 51(1-2), 537-571.

Liu, Y., Hu, Z., Gao, S., Günther, D., Xu, J., Gao, C., Chen, H., 2008. In situ analysis of major and trace elements of anhydrous minerals by LA-ICP-MS without applying an internal standard. Chemical Geology 257(1-2), 34-43.

Liu, Y., Hu, Z., Zong, K., Gao, C., Gao, S., Xu, J., Chen, H., 2010a. Reappraisement and refinement of zircon U-Pb isotope and trace element analyses by LA-ICP-MS. Chinese Science Bulletin 55(15), 1535-1546.

Ludwig, K.R., 2012. User's manual for Isoplot version 3.75–4.15: a geochronological toolkit for Microsoft Excel. Berkeley Geochronology Center Special Publication, Berkeley, California.

Marien, C.S., Hoffmann, J.E., Garbe-Schönberg, C.D., Münker, C., 2019. Petrogenesis of plagiogranites from the Troodos Ophiolite Complex, Cyprus. Contributions to Mineralogy and Petrology 174(4), 35.

Mattinson, J.M., 1976. Ages of zircons from the Bay of Islands ophiolite complex, western Newfoundland. Geology 4(7), 393-394.

493 Ménot, R.P., Peucat, J.J., Scarenzi, D., Piboule, M., 1988. 496 My age of
494 plagiogranites in the Chamrousse ophiolite complex (external crystalline massifs
495 in the French Alps): evidence of a Lower Paleozoic oceanization. Earth and
496 Planetary Science Letters 88(1-2), 82-92.
497 Miyashiro, A., 1973. The Troodos ophiolitic complex was probably formed in an
498 island arc. Earth and Planetary Science Letters 19(2), 218-224.
499 Mukasa, S. B., Ludden, J. N., 1987. Uranium-lead isotopic ages of plagiogranites
500 from the Troodos ophiolite, Cyprus, and their tectonic significance. Geology
501 15(9), 825-828.
502 Niu, Y., Gilmore, T., Mackie, S., Greig, A., Bach, W., 2002. Mineral chemistry, whole
503 -rock compositions, and petrogenesis of Leg 176 gabbros: Data and discussion.
504 In J. H. Natland, et al. (Eds.), Proceedings of the Ocean Drilling Program
505 Scientific Results (Vol. 176, pp. 1–69). College Station, TX: Ocean Drilling
506 Program.
507 Niu, Y.L., O'Hara, M.J., 2003. Origin of ocean island basalts: A new perspective from
508 petrology, geochemistry and mineral physics considerations. Journal of
509 Geophysical Research 108, 2209.
510 Osozawa, S., Shinjo, R., Lo, C.H., Jahn, B.M., Hoang, N., Sasaki, M., Ishikawa, K.,
511 Kano, H., Hoshi, H., Xenophontos, C., Wakabayashi, J., 2012. Geochemistry and
512 geochronology of the Troodos ophiolite: An SSZ ophiolite generated by
513 subduction initiation and an extended episode of ridge subduction?. Lithosphere

514 4(6), 497-510.
515 Pearce, J.A., Robinson, P.T., 2010. The Troodos ophiolitic complex probably formed
516 in a subduction initiation, slab edge setting. Gondwana Research 18(1), 60-81.
517 Piercey, S.J., Murphy, D.C., Mortensen, J.K., Paradis, S., 2001. Boninitic magmatism
518 in a continental margin setting, Yukon-Tanana terrane, southeastern Yukon,
519 Canada. Geology 29(8), 731-734.
520 Regelous, M., Haase, K.M., Freund, S., Keith, M., Weinzierl, C.G., Beier, C., Endres,
521 T., Schmidt, H., 2014. Formation of the Troodos Ophiolite at a triple junction:
522 evidence from trace elements in volcanic glass. Chemical Geology 386, 66-79.
523 Rubatto, D., 2002. Zircon trace element geochemistry: partitioning with garnet and
524 the link between U–Pb ages and metamorphism. Chemical geology 184(1-2),
525 123-138.
526 Schwartz, J.J., John, B.E., Cheadle, M.J., Miranda, E.A., Grimes, C.B., Wooden, J.L.,
527 Dick, H.J., 2005. Dating the growth of oceanic crust at a slow-spreading ridge.
528 Science 310(5748), 654-657.
529 Smith, J.V., 1974. Feldspar Minerals: 2 Chemical and Textural Properties. Springer
530 Science & Business Media, p586.
531 Tilton, G.R., Hopson, C.A., Wright, J.E., 1981. Uranium-lead isotopic ages of the
532 Samail ophiolite, Oman, with applications to Tethyan ocean ridge tectonics.
533 Journal of Geophysical Research: Solid Earth 86(B4), 2763-2775.
534 Warren, C.J., Parrish, R.R., Waters, D.J., Searle, M.P., 2005. Dating the geologic

history of Oman's Semail ophiolite: Insights from U-Pb geochronology. Contributions to Mineralogy and Petrology 150(4), 403-422.

Figure Captions

Fig. 1. Simplified geological map of the Mount Olympus area in the Troodos ophiolite, showing the distribution of plagiogranite and the sample location (34°56'20.83'' N, 32°55'38.69''E, about 1.5 km to the north of the Pano Amiantos village) of this study (modified from Freund et al., 2014).

Fig. 2. Photographs of the plagiogranite. (a) Plagiogranite intruded by diabase; (b) abundant epidote in a hand specimen of the plagiogranite (Sample TDS06); (c) an epidote-free plagiogranite sample consisting of amphibole, plagioclase and quartz (Sample TDS18-08A).

Fig. 3. Representative photomicrographs of plagiogranite in the Troodos ophiolite. (a) Sample TDS18-08B: plagioclase (Pl), quartz (Qtz) and amphibole (Am) in the epidote-free plagiogranite (under plane polarized light; PPL); (b) Sample TDS18-08B: euhedral Am and Qtz with angular shape in the epidote-free plagiogranite (under crossed polarized light; XPL); (c) Sample TDS06: intergrowth of Qtz and skeletal Pl in the epidote plagiogranite (XPL); (d) Sample TDS06: clinopyroxene (Cpx) in the plagiogranite partially altered to chlorite (Chl) (PPL); (e) Sample TDS18-49: euhedral

Pl partially altered to Ep (PPL); (f) Sample TDS18-49: subhedral Qtz surrounded by anhedral Ep crystals and crystal aggregates in the epidote plagiogranites (XPL). BSE images of sample TDS06: (g-h) anhedral zircon (Zrn) in the epidote plagiogranite; (i) most of the titanite (Ttn) crystals in close association with Ep.

Fig. 4. Representative Cathodoluminescence (CL) images of zircon grains from epidote-free plagiogranite (a) and epidote plagiogranite (b, c) of the Troodos ophiolite. Zircons of the epidote-free plagiogranite are euhedral to subhedral with oscillatory zoning, while zircons of epidote plagiogranite are euhedral to anhedral with mottled textures.

Fig. 5. Zircon U-Pb Concordia plots (a-c) and probability diagrams (d-f) of $^{206}Pb/^{238}U$ ages for epidote-free (TDS18-08B) and epidote (TDS06 and TDS18-49) plagiogranite samples of the Troodos ophiolite.

Fig. 6. Ocean crust (Niu and O'Hara, 2003) normalized REE (a, c, e) and multi-element (b, d, f) patterns of zircons in epidote-free (TDS18-08B) and epidote (TDS06 and TDS18-49) plagiogranite samples of the Troodos ophiolite.

Fig. 7. Average composition of zircons of epidote plagiogranite (TDS06, TDS18-49) relative to (divided by) that of zircons of epidote-free plagiogranite (TDS18-08B) in the Troodos ophiolite for REEs (a) and multi-elements (b).

Fig. 8. Ocean crust (Niu and O'Hara, 2003) normalized REE (a, b) and multi-element (c, d) patterns of epidote and titanite in epidote plagiogranite (TDS06) of the Troodos ophiolite.

Fig. 9. Plots of Eu/Eu* vs. Yb_{OCN} (a, b), Yb vs. Zr and Nb (c, d) for epidote and titanite in the epidote plagiogranite (TDS06). Average compositions of plagioclase in gabbro and plagiogranite of the Southwest Indian Ocean Ridge are plotted for comparison (unpublished data). These correlations suggest that compositions of epidote and titanite in the epidote plagiogranite are largely controlled by elemental concentration gradient towards or away from existing crystals (such as plagioclase, zircon, titanite) due to inefficient elemental diffusion during crystallization on microscopic scales.

Fig. 10. Ocean crust (Niu and O'Hara, 2003) normalized elemental patterns for REEs (a) and multi-elements (excluding fluid-mobile elements such as K, Rb, Sr, Ba, U, Pb) (b, c) for plagiogranite of the Troodos ophiolite. Epidote-free plagiogranite from the Troodos ophiolite is highlighted for comparison (Sample Cy 72 from Marien et al., 2019). Plagiogranite data of Main Group and Spilia Group are from Freund et al. (2014) and Marien et al. (2019).

Fig. 11. Plots of (a) Sm/Yb vs. Th/U; (b) Gd/Yb vs. Nb/Ta; (c) Y vs. Eu/Eu*; (d) Y vs. P for zircons in epidote-free (TDS18-08B) and epidote (TDS06 and TDS18-49) plagiogranite samples of the Troodos ophiolite.

Fig. 12. (a) Phase diagram of water by assuming 3.5 wt% NaCl solution like seawater for conceptual clarity and simplicity despite the likely complexity in practice (cannot be constrained) and TDS06 melt in temperature-pressure space. Blue segmented lines show phase boundaries in the H_2O-NaCl system (calculated using SoWat software,

Driesner and Heinrich, 2007). Black line shows wet solidus (melt fraction = 1 wt%) of TDS06 with 3 wt% H_2O content, QFM buffer, and blue line shows corresponding H_2O saturated boundary (calculated using Rhyolite-MELTS, Gualda et al., 2012). The critical point for 3.5 wt% NaCl solution is indicated. The single phase fluid (for H_2O-NaCl system) field at temperatures and pressures above the critical point is supercritical, which can effuse through solids like a gas, and dissolve materials like a liquid, becoming highly hydrous melt or silicic fluids. (b) Schematic model for the genesis of the epidote plagiogranite in the Troodos ophiolite. With decreasing temperature, minerals begin to crystallize, and H_2O in the residual melt gradually becomes saturated. The continued crystallization makes the system to change from a melt-dominated into a fluid-dominated environment. These hydrous melts or magmatic fluids of supercritical property can dissolve the existing minerals like plagioclase and amphibole while precipitating zircon, epidote and titanite. Such fluids can dissolve and transport all the chemical elements with compositional heterogeneity well recorded in the precipitating zircon, titanite and epidote crystals.

Table Caption

Table 1. Summary of textural and compositional characteristics of zircons and the host plagiogranite.

Supplementary Table Captions

Table S1. U-Pb dating results for zircons in plagiogranite of the Troodos ophiolite.

Table S2. Trace element compositions for zircons in plagiogranite of the Troodos ophiolite.

Table S3. Major and trace element compositions for epidote in plagiogranite of the Troodos ophiolite.

Table S4. Major and trace element compositions for titanite in plagiogranite of the Troodos ophiolite.

Table S5. Bulk-rock major and trace element compositions for epidote plagiogranite samples of the Troodos ophiolite.

Table 1. Summary of textural and compositional characteristics of zircons and the host plagiogranite.

Sample	TDS18-08B	TDS06	TDS18-49
Host rock	Epidote-free plagiogranite	Epidote plagiogranite	
Host rock mineralogy	Amphibole, plagioclase, quartz	Plagioclase, quartz, epidote, titanite and minor clinopyroxene	
Size	Length/width ~2-4; 60-200 μm in length	Length/width <2; 50-160 μm in length	
Transparency	Transparent with few inclusions	Translucent with inclusions	
Morphology	Euhedral to subhedral prismatic crystals with clear prisms and pyramids	Euhedral to anhedral tetragonal-dipyramid or stubby tetragonal prism shapes with variably and highly pitted surfaces, indicating the presence of fluid in their parental magma	
CL	Oscillatory zoning, indicating a change of magma composition	Mottled textures with or without oscillatory zoning, indicating the presence of fluid in their parental magma	
Composition	Low Sc, P, Y, Nb, Ta and REEs contents, indicating compositions of their parental magma	High Sc, P, Y, Nb, Ta and REEs contents, indicating compositions of their parental magma	
Th/U	0.3-0.9, indicating magmatic origin	0.4-1.6, indicating magmatic origin	
Nb/Ta	1.1-2.9, indicating relatively low Nb/Ta ratio of their parental magma	1.7-5.7, indicating high Nb/Ta ratio of their parental magma	
U-Pb ages (Ma)	91.0 ± 0.4	91.8 ± 0.7	90.1 ± 0.9

Figure 1

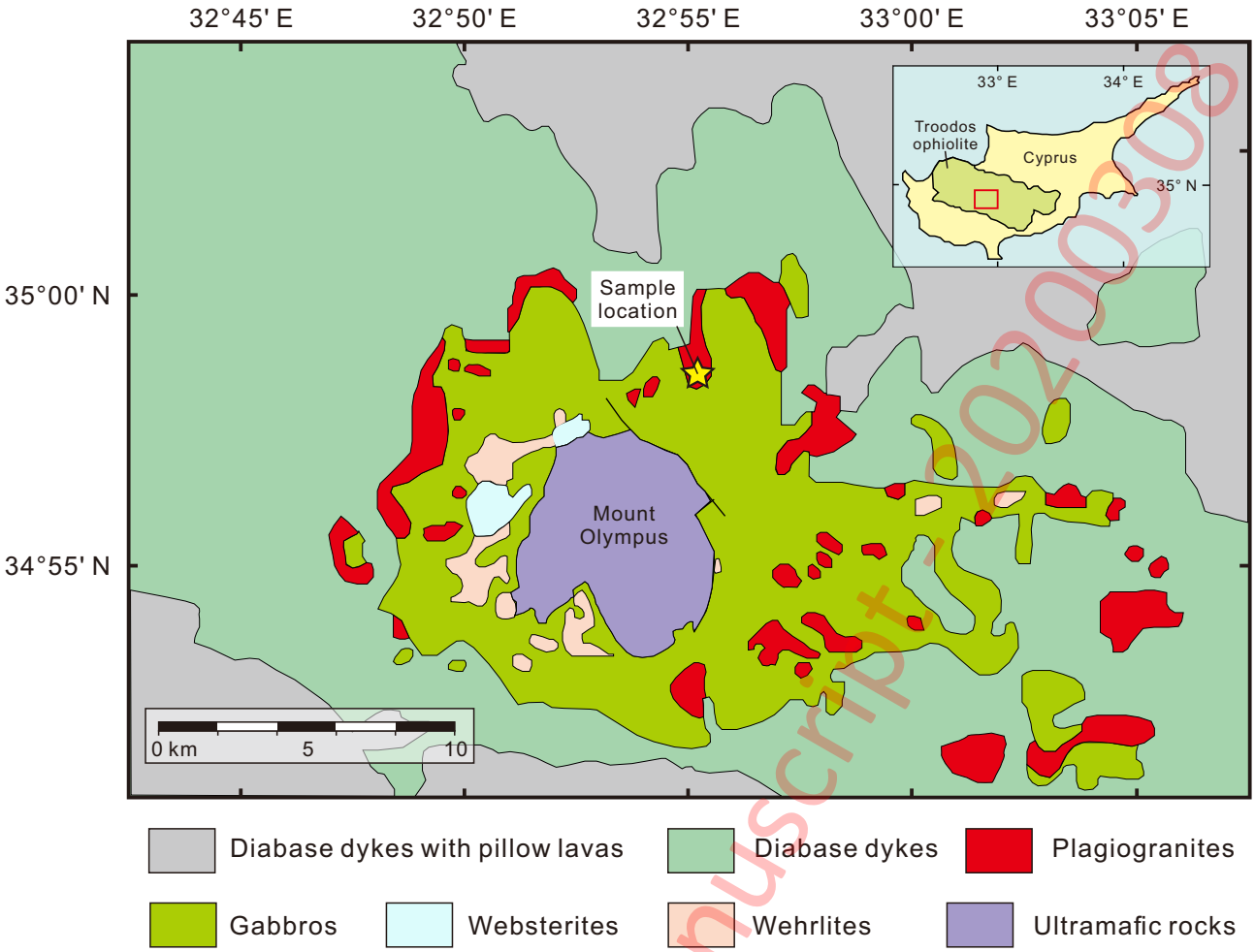

Figure 2

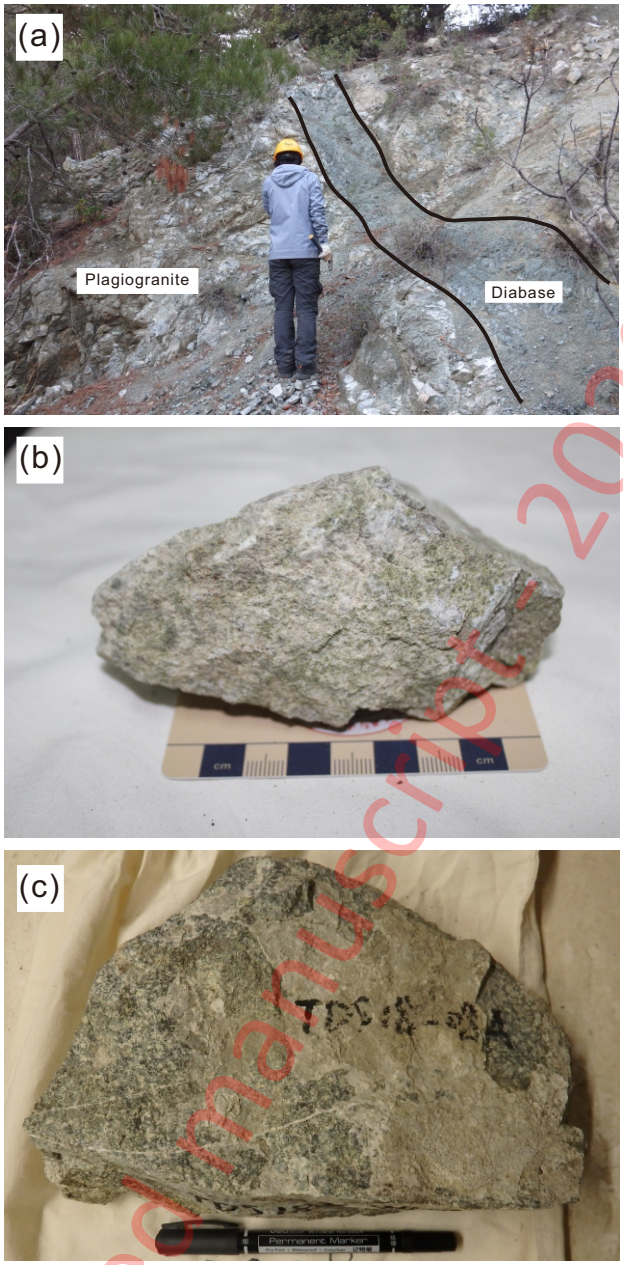

Figure 3

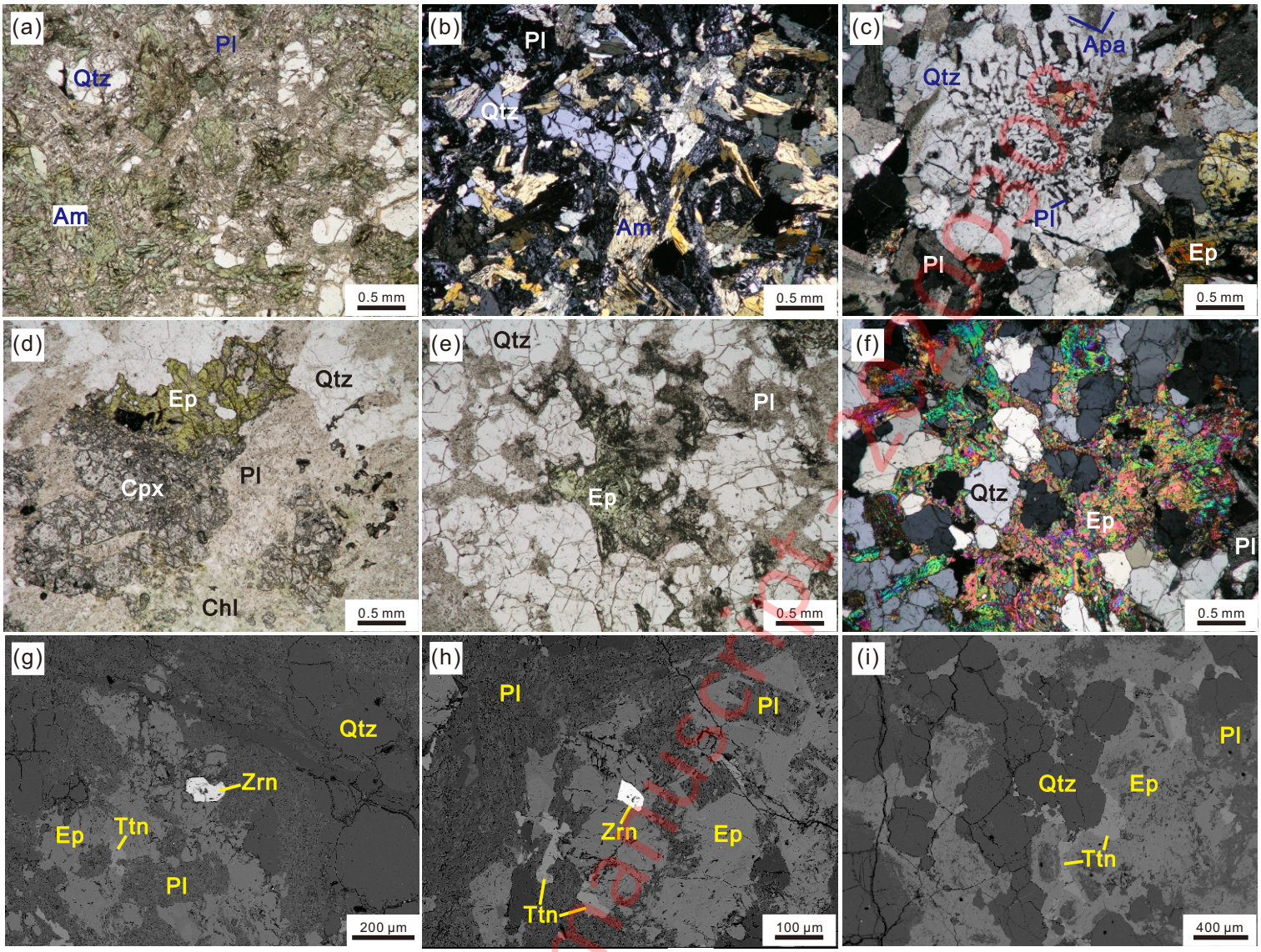

Figure 4

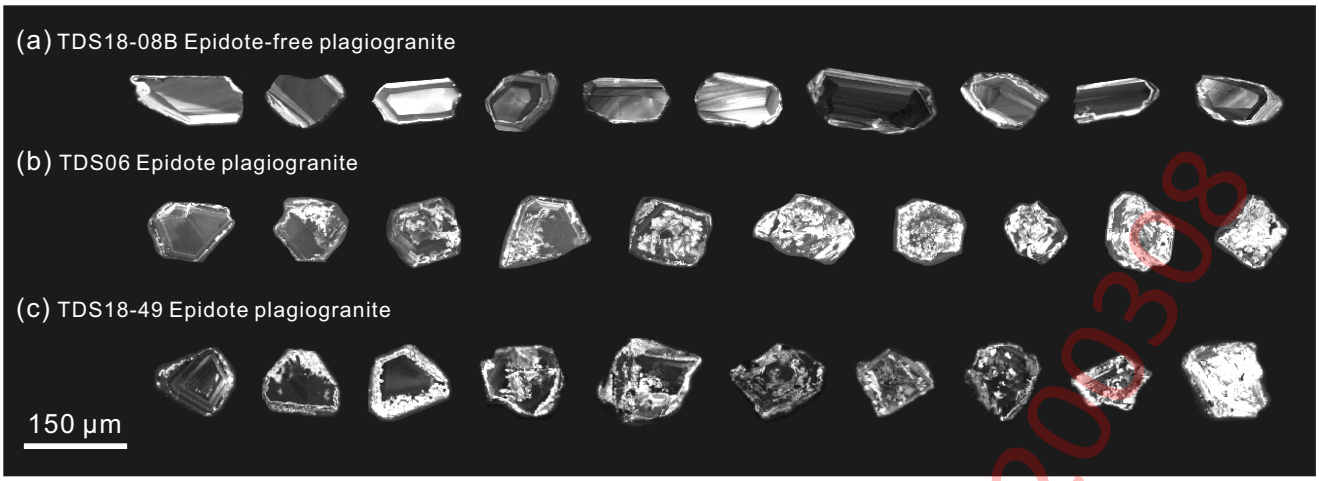

Figure 5

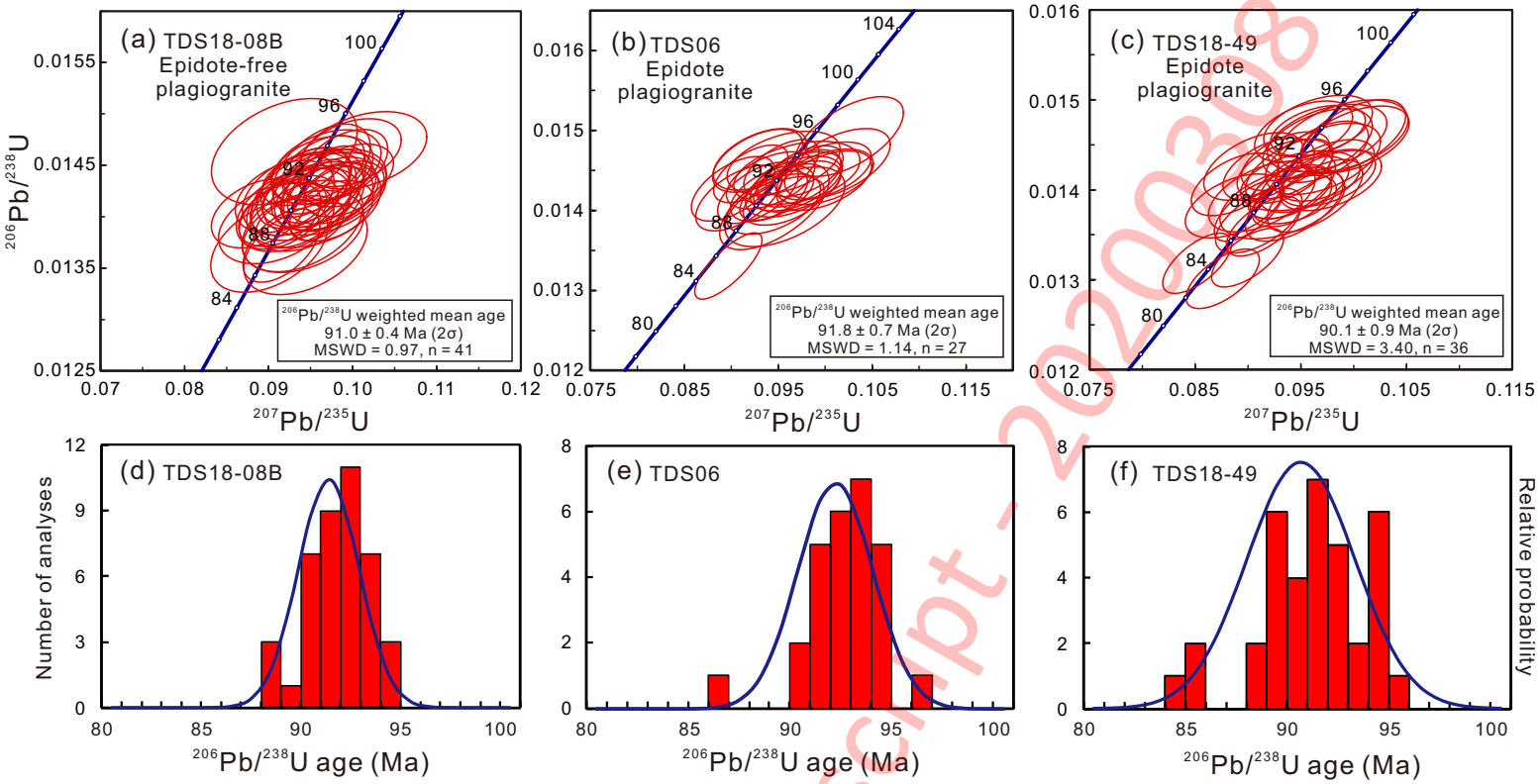

Figure 6

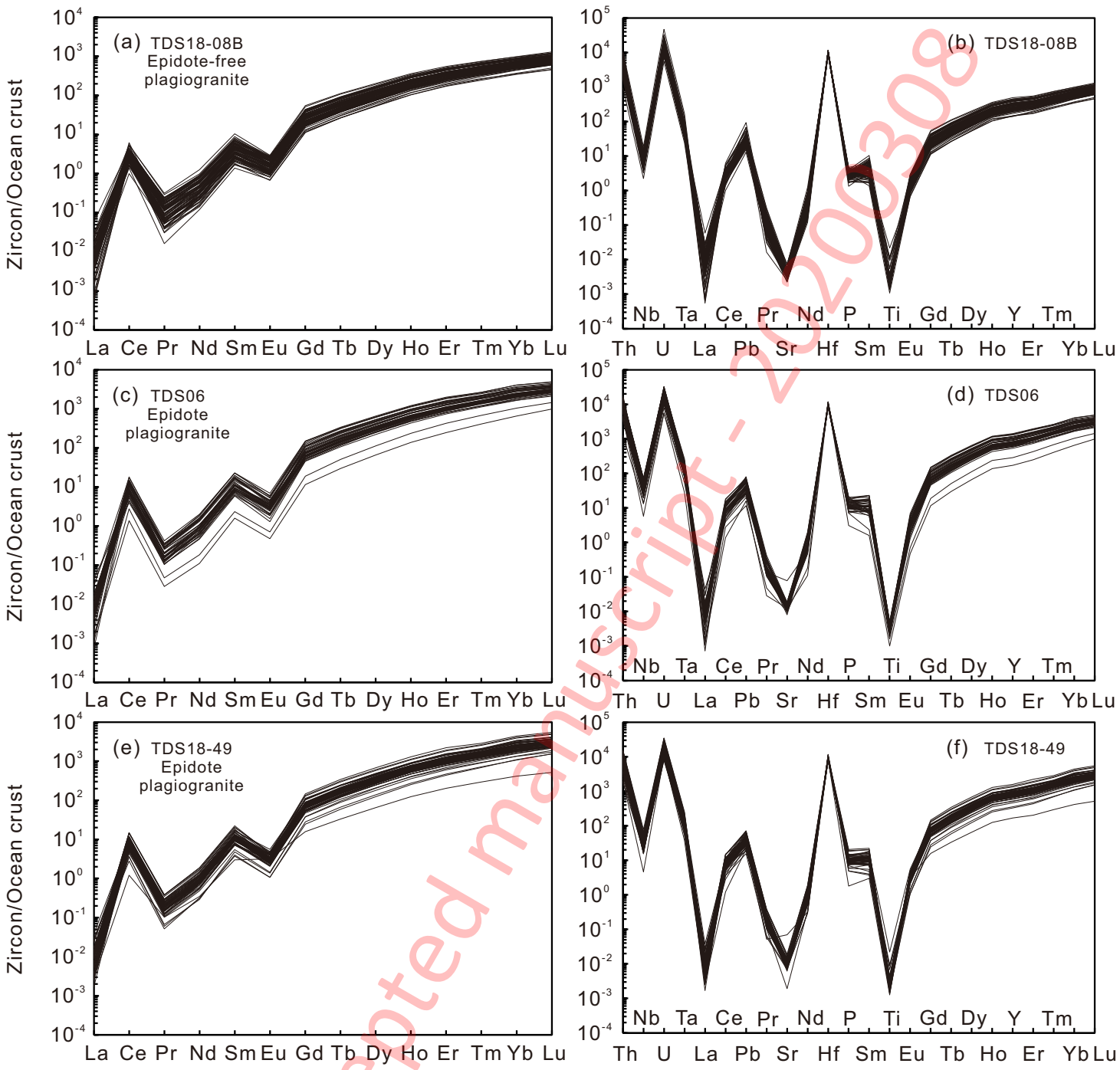

Figure 7

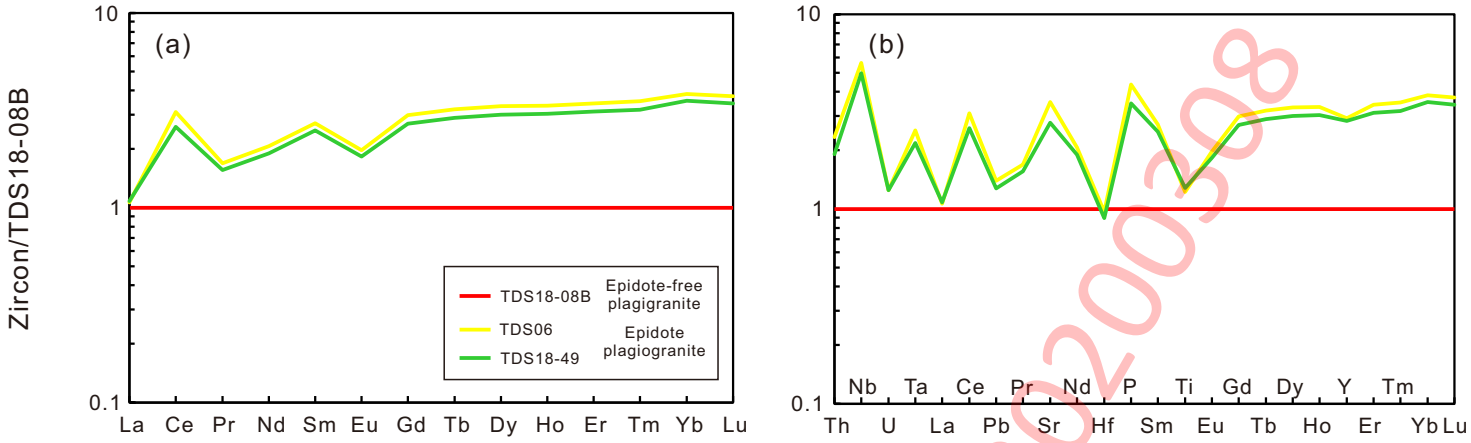

Figure 8

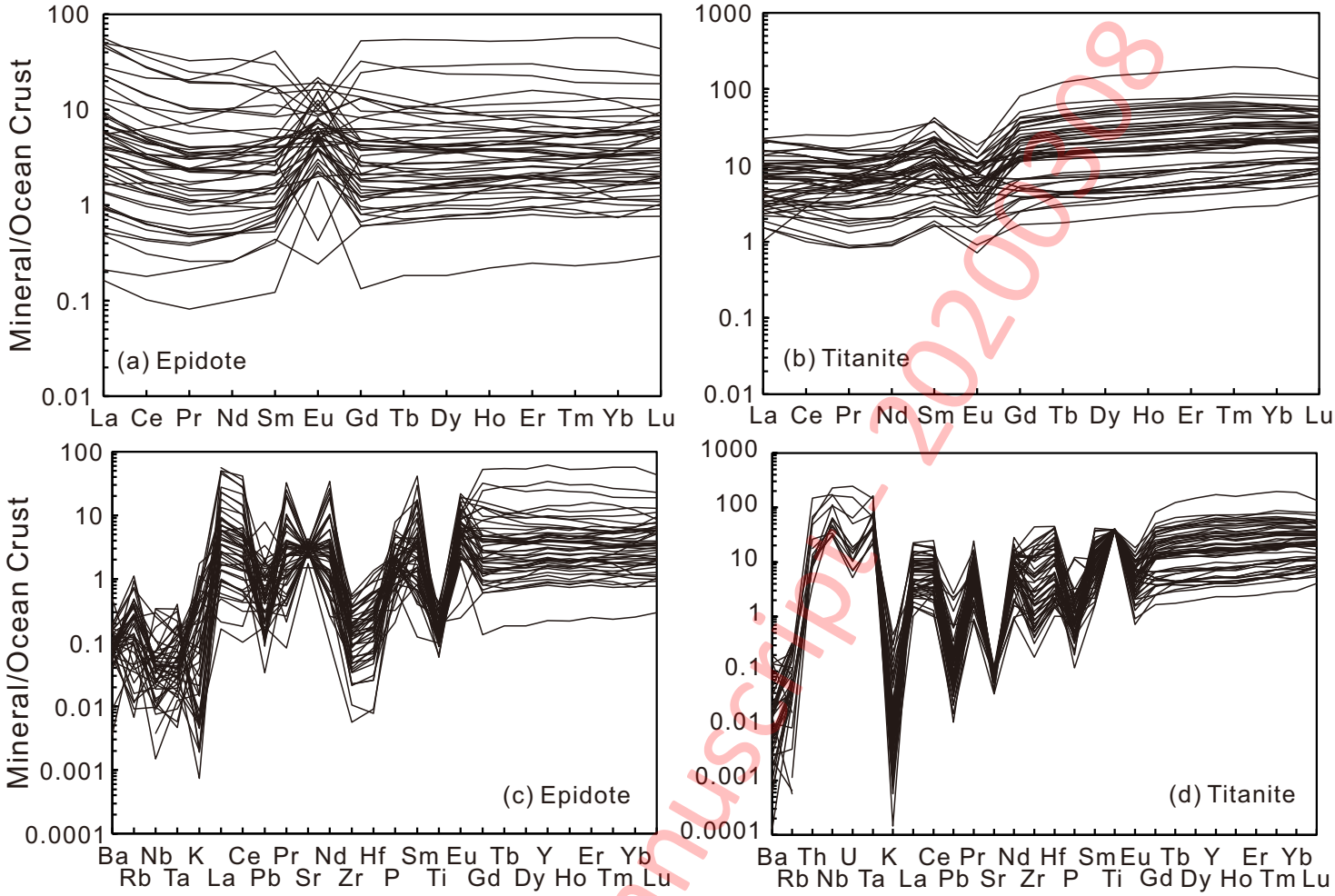

Figure 9

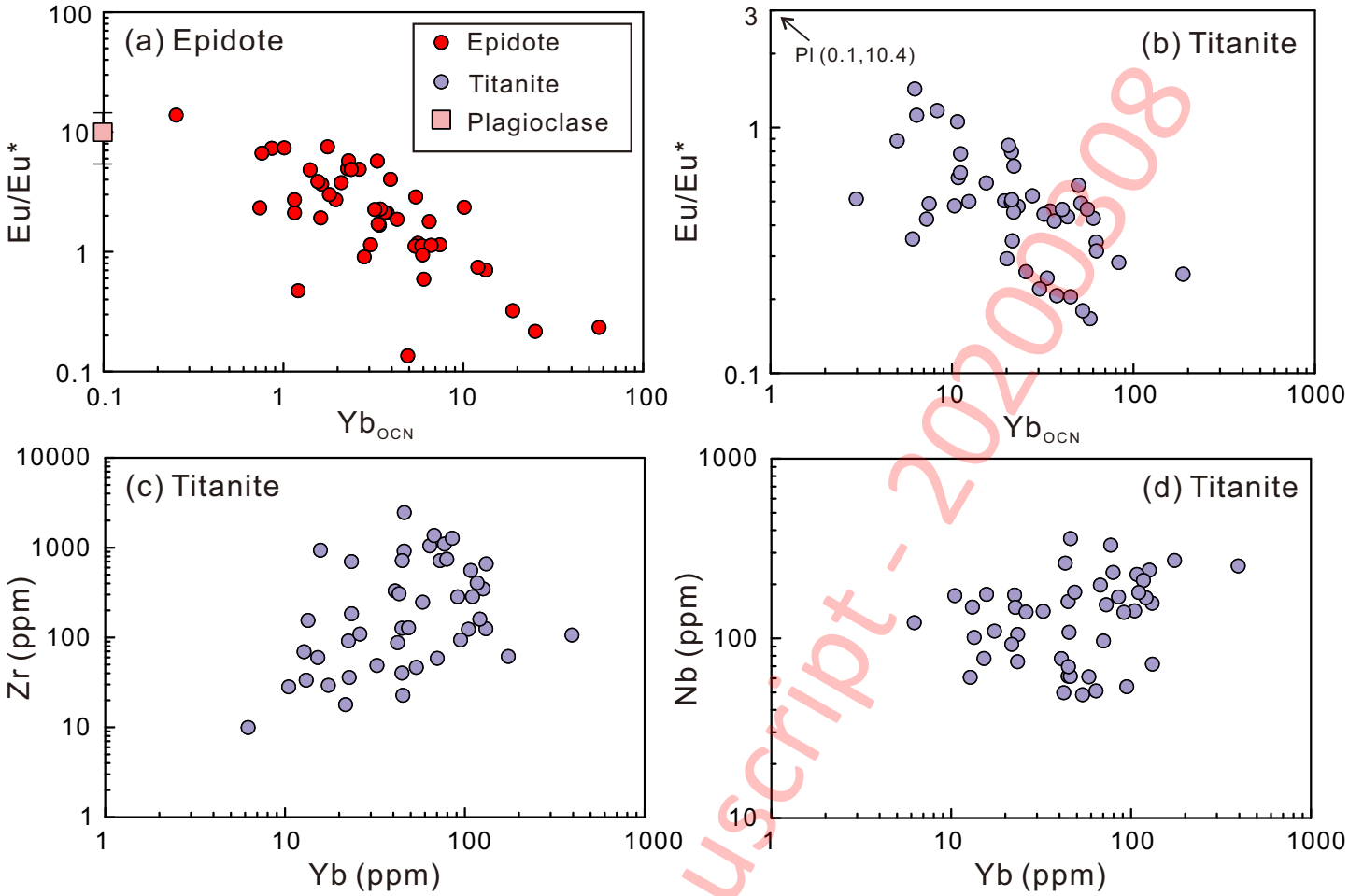

Figure 10

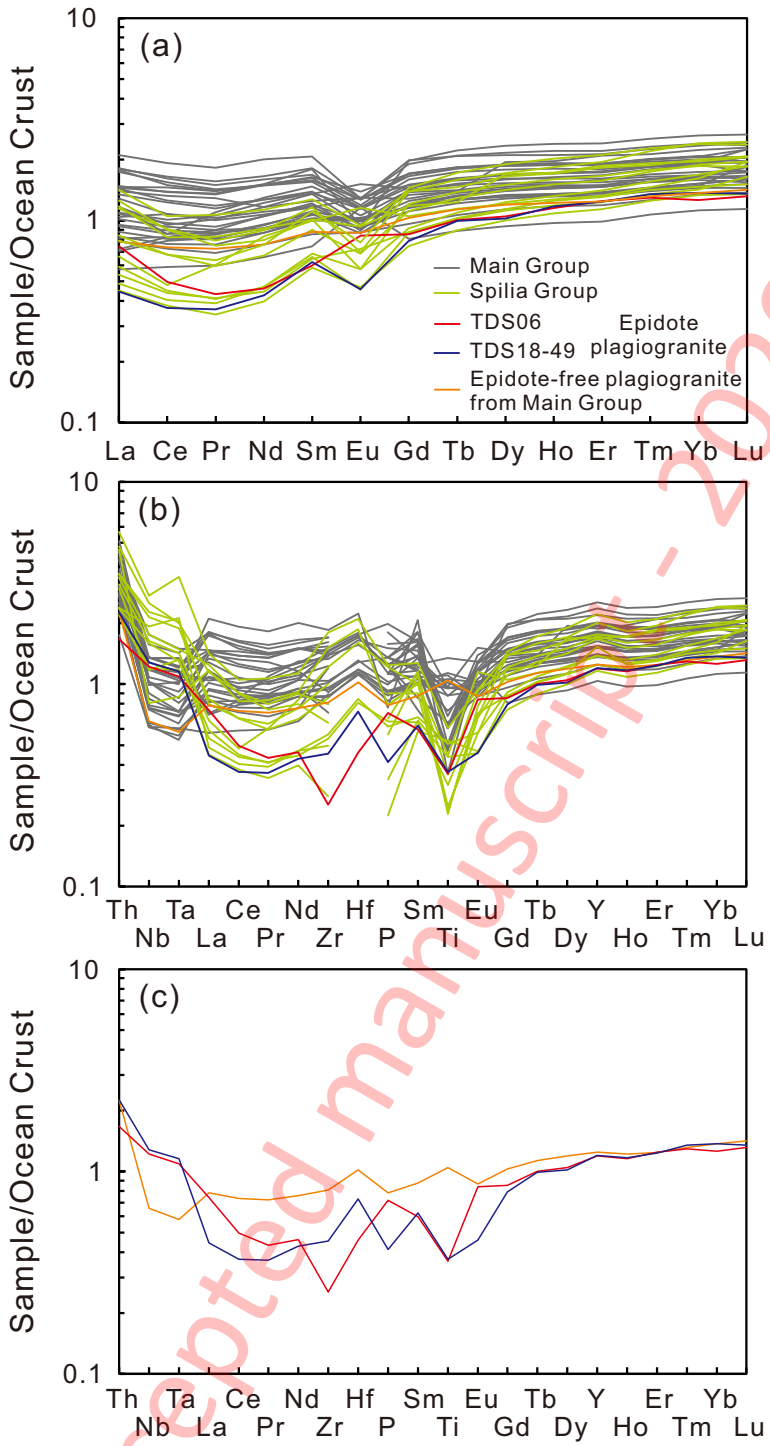

Figure 11

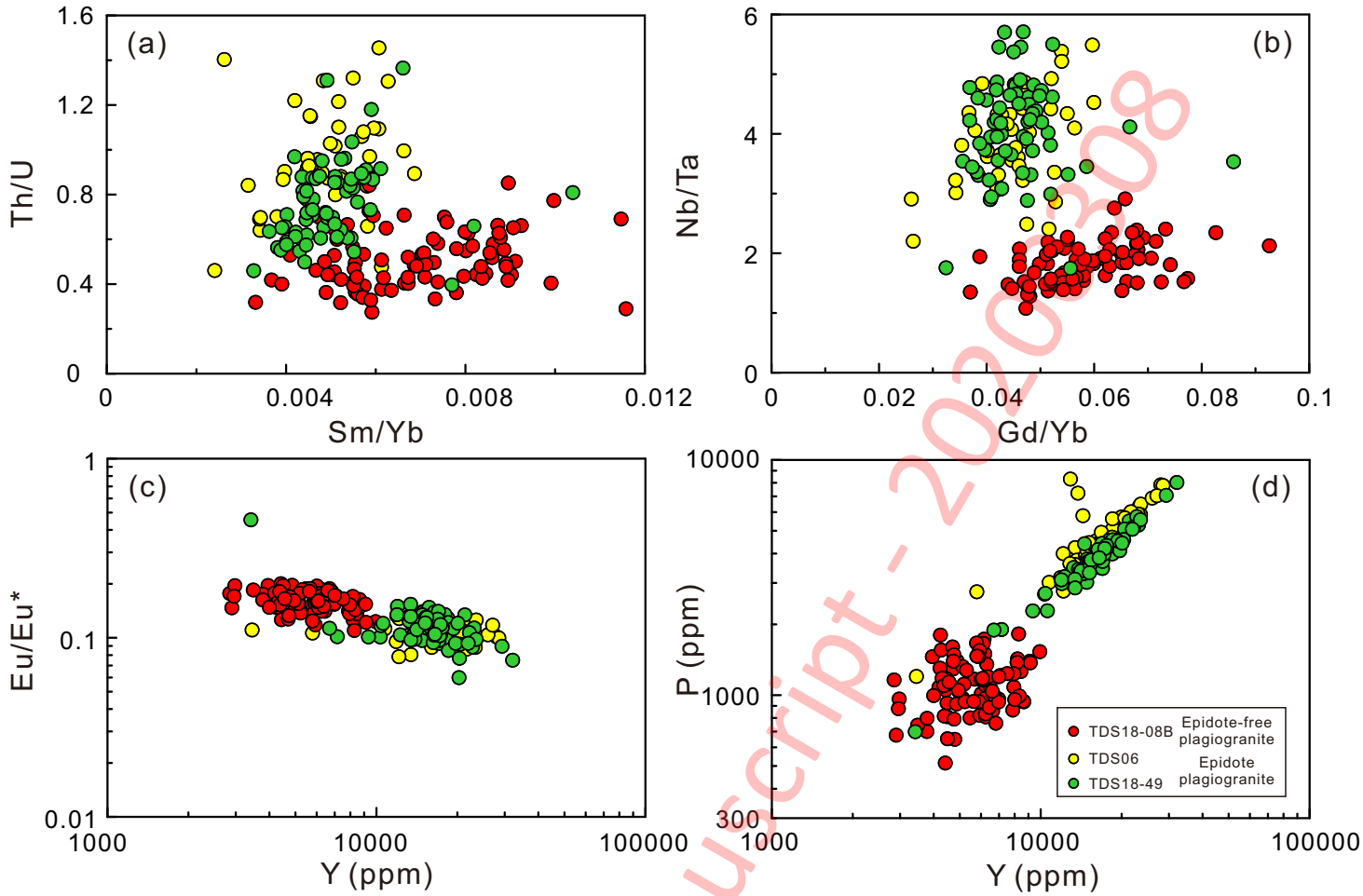

Figure 12